

Article

Numerical Investigation on the Effect of Air Humidification and Oxygen Enrichment on Combustion and Emission Characteristics of Gas Boiler

Haoyu Wang ¹, Xiong Yang ² , Ziyi Li ², Chuanzhao Zhang ^{1,*}, Xianqiang Zhu ³ , Ruijuan Zhang ⁴, Jing Du ¹ and Shuyuan Zhang ¹

- ¹ College of Biochemical Engineering, Beijing Union University, Beijing 100023, China; jdthaoyu@buu.edu.cn (H.W.); djhit2016@163.com (J.D.); 13373778385@163.com (S.Z.)
- ² School of Energy and Environmental Engineering, University of Science and Technology Beijing, Beijing 100083, China; yangx@ustb.edu.cn (X.Y.); ziyili@ustb.edu.cn (Z.L.)
- ³ School of Petroleum and Natural Gas Engineering, Changzhou University, Changzhou 213164, China; zhu@cczu.edu.cn
- ⁴ Beijing Heating Group Shijingshan Branch, Beijing 100042, China; 13810496428@126.com
- * Correspondence: zhangchuanzhao@buu.edu.cn; Tel.: +86-10-5207-2267

Abstract: Gas boilers exhibit thermal inefficiency and unsatisfying pollutant emissions. In this study, numerical simulations were conducted to examine the effect of humidified oxygen-enriched air on methane combustion in a furnace and the effects of different premixed ratios of air on the temperature field inside the furnace, intermediate product OH groups, component concentration distribution, and pollutants. Although humidification of ambient air effectively reduced the flame center temperature and mass concentration of the NO_x generated during combustion in the furnace, the highest growth rate of CO concentration at the furnace outlet was 18.6%. Humidification of oxygen-enriched air increased the center temperature and outlet NO concentration of the furnace compared with those during no oxygen enrichment, but the outlet CO concentration showed a decreasing trend, with the highest decrease rate of 34.6%. This study determined an optimal CO–air premix ratio with a moisture concentration of 50 g/kg dry air and an oxygen concentration of 23%. The air humidification and oxygen enrichment technology proposed in this article provides a technical reference for low nitrogen transformation of existing gas boilers.

Keywords: gas boiler; combustion characteristics; humidity ratio; NO emission reduction



Citation: Wang, H.; Yang, X.; Li, Z.; Zhang, C.; Zhu, X.; Zhang, R.; Du, J.; Zhang, S. Numerical Investigation on the Effect of Air Humidification and Oxygen Enrichment on Combustion and Emission Characteristics of Gas Boiler. *Processes* **2024**, *12*, 2282. <https://doi.org/10.3390/pr12102282>

Academic Editor: Albert Ratner

Received: 11 September 2024

Revised: 11 October 2024

Accepted: 16 October 2024

Published: 18 October 2024



Copyright: © 2024 by the authors. Licensee MDPI, Basel, Switzerland. This article is an open access article distributed under the terms and conditions of the Creative Commons Attribution (CC BY) license (<https://creativecommons.org/licenses/by/4.0/>).

1. Introduction

In recent years, the challenges of thermal inefficiency and pollutant emissions in gas boiler combustion have driven significant advancements in combustion technology worldwide [1,2]. Various techniques such as staged combustion, flue gas recirculation, premixed humidified combustion, flameless combustion, and catalytic combustion have been explored [3]. Among these, premixed humidification and low-NO_x combustion technologies have garnered notable attention due to their potential in reducing pollutant emissions and enhancing efficiency.

Zhang et al. [4] demonstrated through experimental and numerical investigations that humidification in methane flames effectively reduces carbon particulate emissions. Yang et al. [5] employed CFD modeling to analyze temperature distributions and NO_x concentrations in methane and propane flames under varying humidity conditions. Their results showed that moist air combustion significantly reduces nitrogen oxide formation. Shi et al. [6] experimentally analyzed the influence of flue gas recirculation on the combustion characteristics of methane/air mixtures and found that flue gas recirculation technology effectively inhibits the generation of NO_x. Zhang et al. [7] confirmed that the introduction

of humidified air during combustion leads to a significant reduction in NO_x emissions at the furnace outlet.

However, while the reduction in NO_x is promising, several challenges remain unresolved, particularly regarding the combustion stability and the increase in CO emissions. Boushaki et al. [8] noted that increased air humidity reduces both the combustion rate and flame temperature in the furnace chamber, potentially compromising combustion stability. Furthermore, Ge et al. [9] observed that humidified air, while effective in reducing NO_x emissions, contributes to CO concentration fluctuations and incomplete combustion.

A key issue is finding the optimal balance between reducing NO_x emissions and maintaining combustion stability. Yang et al. [10] showed that increasing the excess air coefficient can lower furnace and flue gas temperatures, while Wang et al. [11] compared three diluents—excess air, flue gas, and water vapor—and found that excess air increases NO_x emissions at the stability limit in humidified combustion.

Although recent advances in oxygen-enriched combustion have shown promise for improving combustion performance, particularly in terms of higher temperatures and better fuel utilization [12], the trade-off between increased oxygen levels and the rise in NO_x emissions remains a challenge. Studies by Chen et al. [13] and Ying et al. [14] have further emphasized the complexity of controlling flame propagation and combustion kinetics under varying fuel compositions and oxygen enrichment conditions. Li et al. [15] conducted a numerical investigation using computational fluid dynamics (CFD) to study methane combustion and emissions in a natural gas-diesel dual-fuel engine. The focus was on understanding how methane is consumed during different stages of combustion and identifying the causes of unburned methane emissions. The innovative aspect of this work was the use of CFD to visualize the spatial distribution of methane within the engine cylinder for the first time, providing valuable insights into how methane emissions can be reduced by improving fuel-air mixing and optimizing the pilot fuel injection system. Perpignan et al. [16] focused on modeling pollutant emissions in flameless combustion systems. Using a combination of computational fluid dynamics (CFD) and a chemical reactor network (CRN), the study aimed to predict emissions like nitrogen oxides (NO_x) and carbon monoxide (CO) more accurately. The key innovation lies in integrating detailed chemical reactions into the CRN, reducing computational cost while improving accuracy in emission predictions compared to traditional CFD methods alone. This method enhanced combustion efficiency and emission control. Erfan et al. [17] examined how different turbulence models affect the simulation of swirling combustion. The researchers compared three models: Reynolds stress model (RSM), spectral turbulence analysis, and the RNG $k-\epsilon$ model. They found that RSM with the probability density function (PDF) approach was the most accurate, especially for swirling flows. The study also looked at heat transfer, finding that the discrete ordinate (DO) model was more precise than the P-1 model.

Despite these advances, the gap in current research lies in fully optimizing the air premix ratio for oxygen-enriched and humidified combustion in industrial gas boilers. Most studies focus either on reducing NO_x emissions or improving combustion stability, but few have effectively balanced both objectives. Furthermore, the combined effect of oxygen enrichment and air humidification on NO_x, CO, and soot emissions, particularly under varying premix ratios, remains underexplored.

This study aims to fill this gap by conducting a numerical simulation of oxygen-enriched combustion with air premixing and humidification to identify the optimal air premixing ratio. By analyzing the interactions between combustion temperature and pollutant emissions (NO_x, CO, and soot), this work provides valuable insights into the low-NO_x transformation of gas boilers. The findings offer a practical strategy for reducing emissions while maintaining combustion stability, addressing the dual challenge of environmental impact and energy efficiency in industrial applications.

2. Mathematical Model and Boundary Conditions

2.1. Geometric Models and Control Equations

A simplified representation of the gas boiler structure was adopted, focusing on a half-axisymmetric model of the cylindrical combustion chamber for 3D simulation, as shown in Figure 1. The fuel is introduced through the central nozzle of the burner, which has a length of 0.02 m and a diameter of 0.002 m. The surrounding annular region supplies the secondary gas, which mixes with the methane fuel before combustion occurs. The main geometry parameters are listed in Table 1.

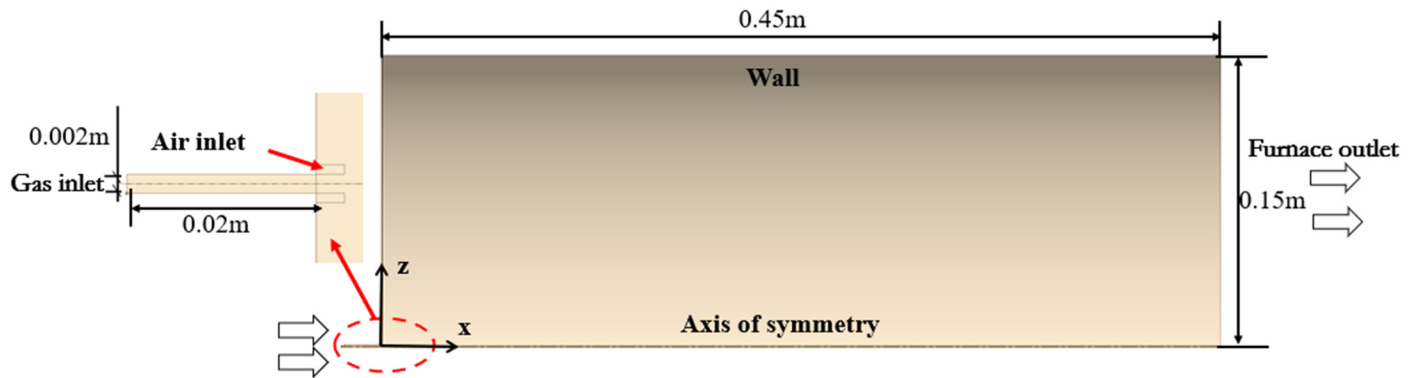


Figure 1. Boiler structure.

Table 1. The main geometry parameters.

Parameter	Value
Gas inlet length/m	0.02
Gas inlet diameter/m	0.002
Air inlet length/m	0.003
Air inlet diameter/m	0.002
Boiler length/m	0.45
Boiler diameter/m	0.15

The general form of the Eulerian transport equation used was as follows [18,19]:

$$\frac{\partial}{\partial x}(\rho u \varphi) + \frac{\partial}{r \partial r}(r \rho v \varphi) + \frac{\partial}{r \partial \theta}(\rho w \theta) = \frac{\partial}{\partial x} \left| \Gamma_{\varphi} \frac{\partial \varphi}{\partial x} \right| + \frac{\partial}{r \partial r} \left| r \Gamma_{\varphi} \frac{\partial \varphi}{\partial r} \right| + \frac{\partial}{r^2 \partial \theta} \left| r \Gamma_{\varphi} \frac{\partial \varphi}{\partial \theta} \right| + S_{\varphi}, \quad (1)$$

where ρ is the calculating fluid density, kg/m^3 , φ is the universal dependent variable, Γ_{φ} is the diffusion coefficient, S_{φ} is a source term, and x , r , θ are axial coordinates, radial coordinates, and circumferential coordinates, respectively. u , v , w are the components of the velocity vector in the x , r , θ directions respectively, m/s . When $\varphi = 1$ and $\Gamma_{\varphi} = 0$, the relationship is the continuity equation. When $\varphi = u$, v , w , it is the momentum equation corresponding to the x , r , θ directions, respectively. $\varphi = k$ is the turbulent kinetic energy equation, and $\varphi = \varepsilon$ is the turbulent flow energy dissipation rate equation. $\varphi = f$ is the conservation equation of components. $\varphi = h$ is the energy equation. K is turbulent energy, ε is turbulence dissipation, f is the mass fraction, %, and h is the enthalpy value, J/kg .

2.2. Numerical Methods

A realizable k - ε two-equation model with a scalable wall function was chosen to simulate turbulence. The discrete ordinates (DO) model was employed for radiative heat transfer. All wall boundaries were set as adiabatic, non-slip conditions. The steady-state diffusion flame model from the non-premixed combustion framework was selected for the fuel and oxidizer interaction. A simplified methane gas-phase chemical reaction mechanism was assumed [20,21]. Gas-phase kinetics and thermodynamic data were imported into

Fluent using Chemkin. The NO_x formation was modeled using both the thermal NO_x and prompt NO_x mechanisms (F2–F8). For soot modeling, the two-step soot model in Fluent was employed, accounting for the interaction between soot and radiation [22].

The relevant reactions were as follows:

Thermal NO_x formation:



Prompt NO_x formation:



2.3. Mesh Independence Validation

CFD commercial software was utilized for meshing the burner (Figure 2). To predict the combustion characteristics more accurately inside the boiler, local mesh refinement was applied at the fuel and air inlets, while boundary layer meshing was implemented along the furnace walls. Coarser mesh was used in other regions to optimize computational efficiency. The computational domain was discretized and analyzed for grid independence. The following five grid cell counts were considered: 176,393, 192,761, 206,351, 225,127, and 262,090. The grid independence verification results are shown in Figure 3. When the number of cells was increased to 206,351, the average temperature at the furnace outlet remained essentially constant, indicating grid independence. Therefore, to balance computational efficiency and accuracy, 206,351 cells were chosen for the final calculation.

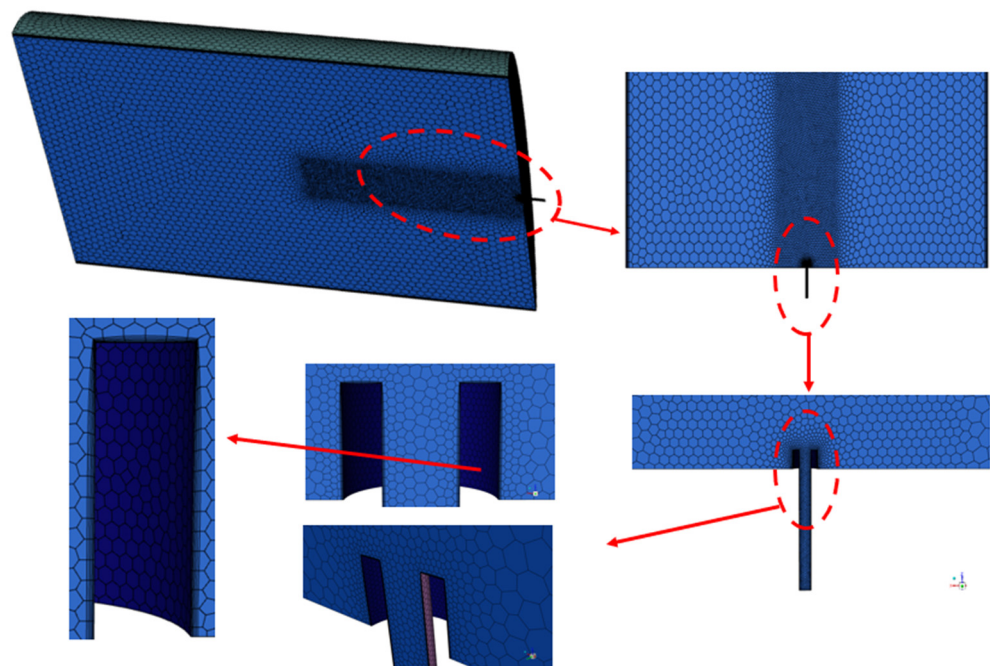


Figure 2. Detailed mesh of the model.

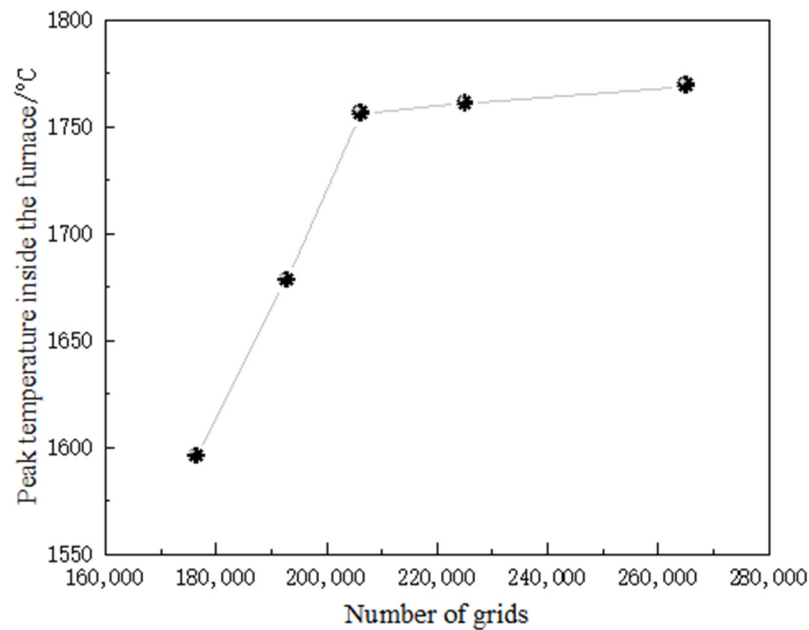


Figure 3. Peak temperature inside the furnace at different grid numbers.

2.4. Initial and Boundary Conditions

The simulation process utilized a velocity inlet as the inlet boundary condition, with the mole fractions of fuel and air determined based on different equivalence ratios. The outlet boundary condition was defined as a pressure outlet. Adiabatic boundary conditions were applied to the front and rear wall surfaces corresponding to the inlet and outlet of the combustion chamber. When considering heat transfer, both radiation and convective heat transfer between the combustion chamber walls and the surrounding environment were accounted for.

The pressure-based COUPLED algorithm was employed to solve the governing equations and calculate the flow field. To improve gradient calculations, an element-based approach was used, incorporating least squares, standard pressure, and second-order upwind schemes for momentum, species components, and energy equations. The specific boundary conditions are listed in Table 2. High-purity oxygen (with a purity exceeding 95%) was generated using a pressure swing adsorption (PSA) system. This oxygen was blended with air in controlled ratios to produce a combustion-supporting gas with the desired oxygen concentration. The mixture was introduced into the furnace along with the fuel, where combustion occurred similarly to conventional combustion systems, completing the heat transfer process. The simulation conditions, including 11 different air humidity ratios and oxygen concentrations, are summarized in Table 3.

Table 2. Boundary and initial conditions of the calculation model.

Boundary	Parameter	Temperature/K	Velocity/ (m·s ⁻¹)	Turbulence Intensity/%	Hydraulic Diameter/m
Air inlet	Velocity (m/s)	373	0.2	10	0.144
Gas inlet	Velocity (m/s)	373	64	10	0.002
Wall	No slip	300	-	-	-
Pressure outlet	Gage pressure (MPa)	300	-	10	0.3

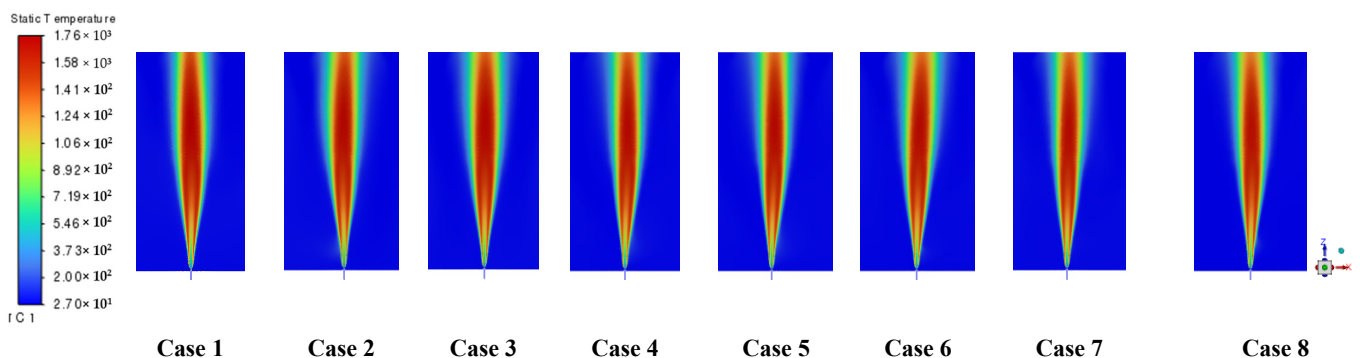
Table 3. Eleven humidity ratios of air and oxygen concentration.

Case	Combustion		Fuel Velocity (m s^{-1})
	Humidity Ratio of Air (g/kg dry air)	O_2 Concentration (vol %)	
1	7	21%	64
2	21	21%	64
3	42	21%	64
4	50	21%	64
5	75	21%	64
6	100	21%	64
7	125	21%	64
8	150	21%	64
9	50	22%	64
10	50	23%	64
11	50	24%	64

3. Numerical Simulation Results

3.1. Combustion Characteristics and Nitrogen Reduction Effect of Air Humidification

Temperature is a key indicator of the combustion process within the furnace chamber [23]. Figure 4 presents the combustion temperature distribution at various air humidity ratios. Although the overall characteristics of the temperature distribution remained similar across the different humidity levels, the high-temperature region was consistently concentrated near the central axis of the furnace chamber. As the humidity ratio increased, the temperature in this high-temperature region gradually decreased. For instance, at a humidity ratio of 7 g/kg dry air, the highest combustion temperature reached 1756 K, while the furnace outlet temperature was 1388 K (Figure 4). When the humidity ratio increased to 150 g/kg dry air, the peak combustion temperature dropped to 1689 K, with the outlet temperature decreasing to 1266 K. The overall temperature reduction from Case 1 to Case 8 was 3.8%. This reduction is attributed to the heat absorbed by the water vapor during evaporation, as water vapor has a higher specific heat capacity compared to oxygen and nitrogen. Consequently, humidifying the air lowers the central flame temperature, which indirectly reduces the intensity of the chemical reactions within the furnace chamber.

**Figure 4.** Regional distribution of temperature under different humidity ratios of air.

Cloud view of CO distribution with different excess air factors.

In the combustion study, the combustion reaction zone contained a large amount of OH radicals. The OH radical density can be used to characterize the flame reaction zone and its reaction characteristics, which can subsequently be used to diagnose the combustion effect [24]. The distribution of the OH radical mass fraction under different humidity ratios of air is shown in Figure 5. The concentration of OH radicals in the formation zone increased gradually with the humidity ratio of air. This was observed because the reaction in which water vapor is mainly involved generates a larger amount of OH radicals

(Equations (2) and (3)) with increasing humidity ratio of air, which affects the consumption of OH, thereby increasing the concentration of OH inside the boiler.

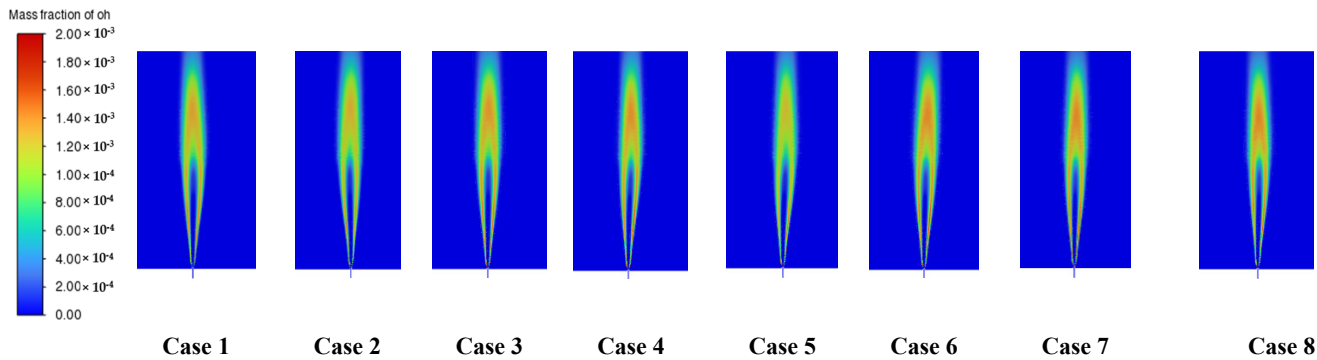


Figure 5. Regional distribution of OH group mass fraction under different humidity ratios of air.

Current research on boiler emission pollutants indicates that approximately 90% of the NO_x produced in turbulent jet flames is in the form of NO [25–28]. Figure 6 illustrates the thermal NO_x generation rate at various humidity ratios of air. The generation rate of thermal NO_x in the high-temperature zone at the center of the combustion flame decreased as the moisture content in the air increased. In Case 1, where the air had the lowest humidity ratio, the center of the combustion flame exhibited the darkest regions, indicating the highest thermal NO_x generation rate. This stratification in NO_x generation occurred because the combustion temperature in the furnace reached levels that promote thermal NO_x formation. At a humidity ratio of 7 g/kg dry air, the peak NO_x generation rate in the furnace chamber was 5.88×10^{-6} kg/(m³ s). However, as the humidity ratio increased to 150 g/kg dry air, the maximum NO_x generation rate dropped to 1.47×10^{-6} kg/(m³ s). This confirms that the NO_x generation rate decreases as the air's moisture content increases, likely due to the cooling effect of water vapor, which reduces the peak combustion temperatures that drive thermal NO_x formation.

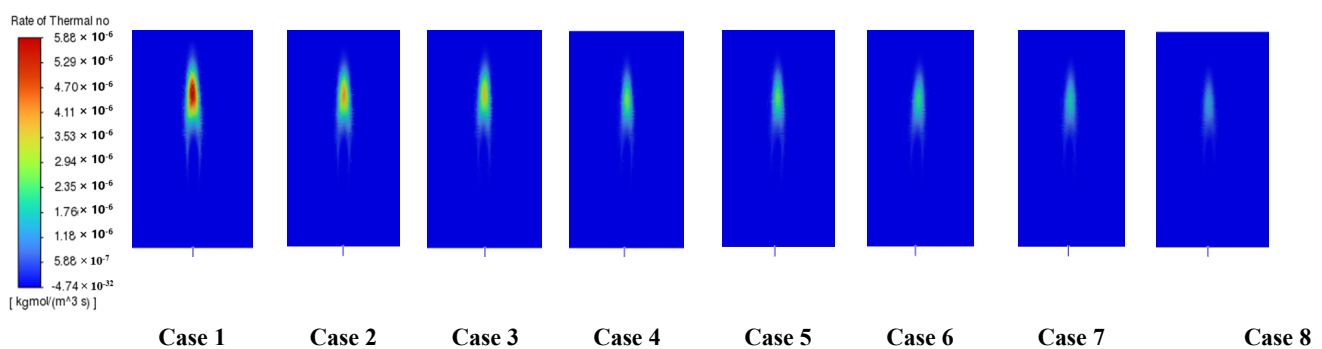


Figure 6. Regional distribution of thermal NO_x under different humidity ratios of air.

Figure 7 presents the NO concentration at the outlet under varying air humidity ratios. NO, being the primary component of NO_x in gas boilers, forms as a result of the high-temperature reaction between nitrogen and oxygen, particularly under conditions of oxygen enrichment. As illustrated, NO emissions decrease by approximately 70% when the air humidity ratio increases from 1.7% to 19.4%, with a noticeable delay in the outlet NO concentration. The primary reason for this reduction is the introduction of humidified air into the combustion zone, where the water vapor mixes with the fuel. As the humidity ratio rises, the peak flame temperature decreases significantly, which suppresses thermal NO_x

formation and leads to a reduction in NO emissions at the outlet. This clearly demonstrates the advantages of humidified combustion in minimizing NOx emissions.

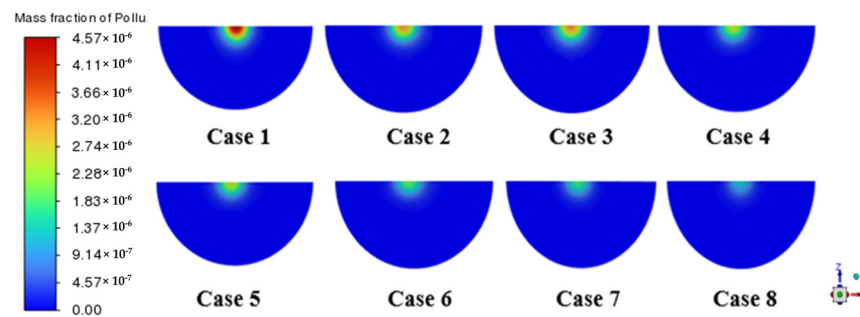


Figure 7. Regional distribution of NO concentration at the outlet under different humidity ratios of air.

Although air humidification technology effectively reduces the average NO concentration at the furnace outlet, it inevitably leads to incomplete combustion and reduced stability [29]. Figure 8 illustrates the CO concentration at the outlet under different air humidity ratios. As the humidity ratio of the air increased, the CO concentration at the furnace outlet also rose. When the humidity ratio of the air was 20 g/kg dry air, the CO mass fraction at the outlet was 0.0458%. At a humidity ratio of 100 g/kg dry air, the CO mass fraction increased to 0.0512%. A sharp increase in CO concentration was observed when the humidity ratio reached 50 g/kg dry air, with the highest growth rate of 18.6%. This rise can be attributed to the impact of oxygen concentration and residence time in the furnace on CO formation. As the humidity ratio increased, the oxygen concentration in the furnace decreased, leading to a reduction in the flame temperature at the combustion center. At the same time, the increased flow velocity shortened the fuel's residence time in the furnace, hindering the complete oxidation of CO and resulting in incomplete combustion. Consequently, a humidity ratio of 50 g/kg dry air was identified as the upper limit for stable gas boiler operation. Further increases in the humidity ratio were found to compromise the stability and efficiency of the boiler [30–32].

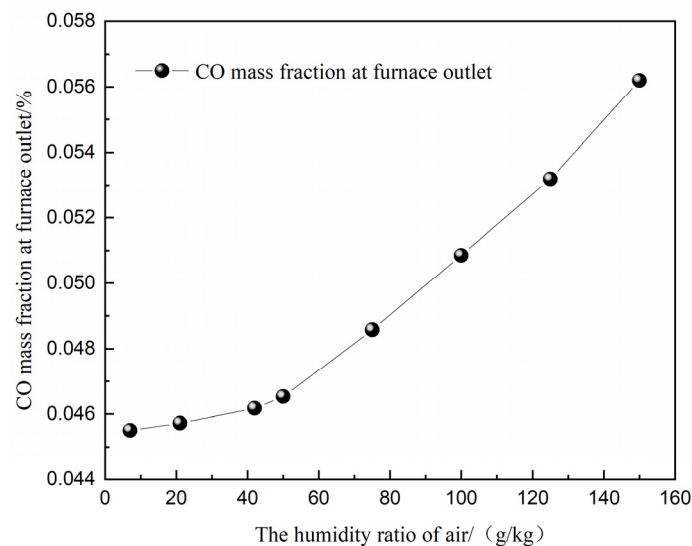


Figure 8. Regional distribution of CO concentration at the outlet under different humidity ratios of air.

3.2. Combustion Characteristics of Air Humidification and Oxygen Enrichment

The optimal air premix ratio must be determined to ensure complete combustion in the furnace chamber, maintain stable boiler operation, and reduce NO emissions at the furnace outlet. To achieve this, a humidity ratio limit of 50 g/kg dry air was set, and the

effect of oxygen enrichment on combustion performance was investigated. Figures 9 and 10 present the impact of varying air oxygen concentrations on furnace temperature and NO emissions at a humidity ratio of 50 g/kg dry air.

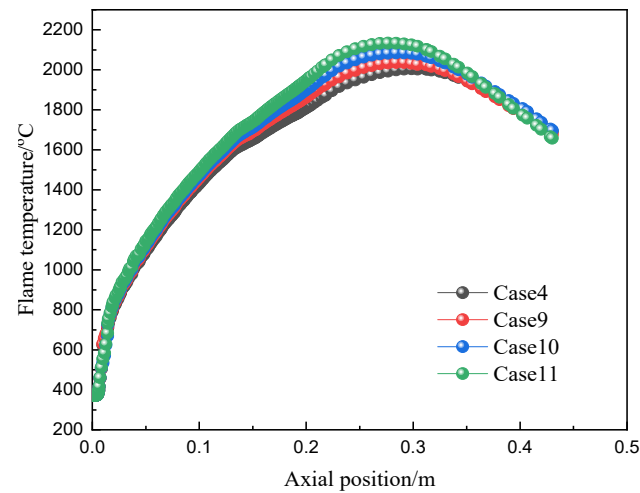


Figure 9. Effect of changes in air oxygen concentration (50 g/kg dry air) on the temperature.

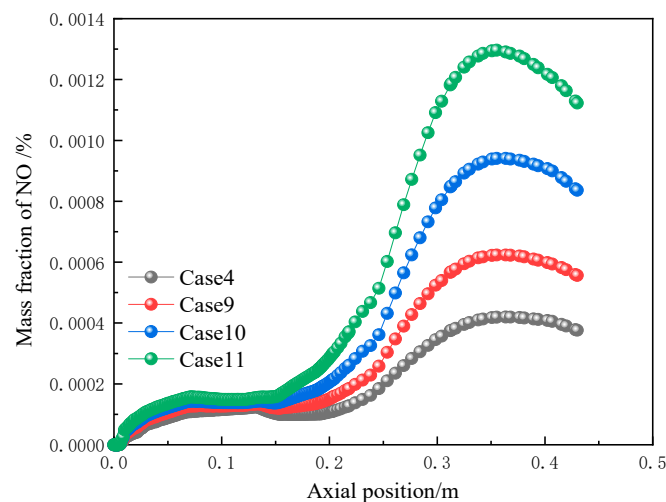


Figure 10. Effect of changes in air oxygen concentration (50 g/kg dry air) on the variation of NO.

The temperature and NO concentration within the furnace increased as the air oxygen concentration rose. Specifically, at oxygen concentrations of 21%, 22%, 23%, and 24%, the maximum axial temperatures in the furnace chamber were 2005 °C, 2037 °C, 2085 °C, and 2133 °C, respectively. The corresponding temperature increases compared to unenriched conditions were 1.6%, 2.3%, and 2.3%, respectively. This increase in temperature is due to the higher oxygen concentration enhancing combustion efficiency, leading to more complete combustion and elevated furnace temperatures, which in turn promote the formation of thermal NO_x and result in higher NO emissions at the furnace outlet.

As the oxygen concentration rose from 21% to 22%, 23%, and 24%, the NO emissions increased by 22%, 33%, and 32.7%, respectively. This highlights the trade-off between increasing oxygen and humidity in the air. While a higher humidity ratio effectively reduces NO emissions in the furnace, increasing the oxygen concentration conversely boosts NO formation due to the higher combustion temperatures.

Figure 11 illustrates the variations in CO concentration and soot mass fraction at the furnace outlet under different oxygen concentrations, with the humidity ratio fixed at 50 g/kg dry air. As the oxygen concentration increased, the CO concentration at the

furnace outlet showed a declining trend, with reduction rates of 7.9%, 12%, and 14.7%, respectively, which enhanced the combustion stability and completeness.

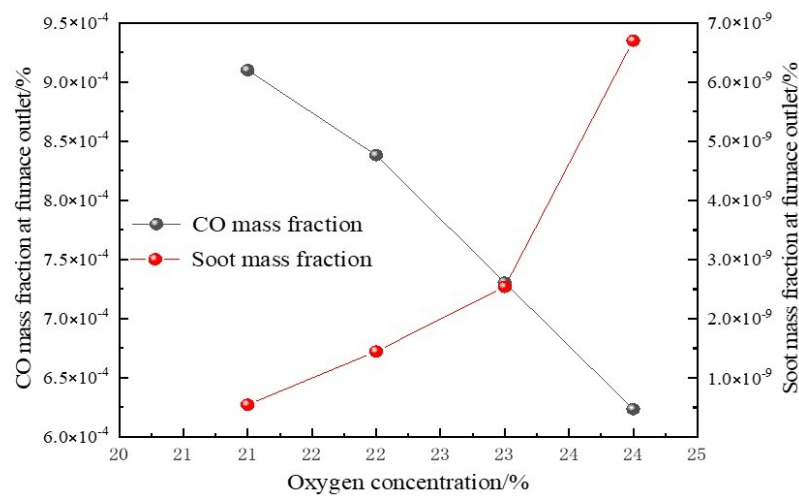


Figure 11. Effect of the variation in oxygen concentration (50 g/kg dry air) on the CO mass fraction and soot mass fraction at the furnace outlet.

Conversely, the soot mass fraction increased with higher oxygen concentrations. This is because the distribution of the soot volume fraction is significantly influenced by the air's oxygen content. The elevated oxygen levels intensified the diffusion of oxygen at key positions, accelerating the combustion process and advancing the soot formation point. Although higher oxygen concentrations reduced the CO mass fraction at the outlet, ensured complete combustion, and kept the soot concentration within permissible atmospheric emission standards, it also caused a slight increase in soot formation.

Based on these observations, the optimal air premixing ratio was determined to be a 50 g/kg dry air humidity ratio combined with 23% oxygen concentration, which balanced efficient combustion with acceptable emission levels.

The increase in soot mass fraction at furnace outlet when oxygen concentration is elevated can be attributed to several factors:

Flame temperature increase: Higher oxygen concentrations can lead to an increase in flame temperature, which promotes the formation of soot precursors due to enhanced pyrolysis of hydrocarbons. In certain regions of the combustion chamber, local oxygen might still be insufficient to fully oxidize the increased soot formation.

Localized oxygen deficiency: Although the overall oxygen concentration is higher, localized regions within the flame may experience oxygen deficiency due to incomplete mixing or high flame temperatures, allowing for increased soot production in these areas.

Radiative heat loss: The elevated flame temperature caused by higher oxygen levels increases radiative heat transfer, potentially leading to local cooling and less effective oxidation of soot particles.

4. Conclusions

The results of this study have several future applications in industrial combustion processes, particularly in optimizing gas boiler performance and reducing pollutant emissions. The combination of air humidification and oxygen enrichment offers a feasible and highly efficient method for achieving lower NO_x emissions while maintaining combustion stability, making it a valuable approach for the retrofit and upgrade of existing boiler systems. The findings highlight practical solutions for improving gas-fired industrial boiler efficiency and emission control. This approach can be applied to pollution control systems, retrofitting older infrastructure, and supporting sustainable energy systems, such as hybrid fuel combustion, aligning with environmental regulations, and reducing carbon footprints. The specific results are as follows:

- (1) The humidity ratio of air effectively reduces the flame center temperature and the NO_x mass fraction generated during combustion in the furnace. When the humidity ratio increases from 7 g/kg dry air to 150 g/kg dry air, the temperature and NO_x reduction rates reach 3% and 70%, respectively. However, the CO fraction at the furnace outlet increases significantly, with the highest growth rate observed at 18.6%. The maximum recommended humidity ratio of air is 50 g/kg dry air.
- (2) The center temperature and NO concentration at the outlet are higher in an oxygen-enriched furnace with air humidification compared to non-enriched conditions. When the humidity ratio is 50 g/kg dry air and the oxygen concentration increases from 21% to 22%, 23%, and 24%, the temperature growth rates are 1.6%, 2.3%, and 2.3%, respectively. Correspondingly, the NO concentration increases by 22%, 33%, and 32.7%. In contrast, the CO concentration at the furnace outlet decreases, with reduction rates of 7.9%, 12%, and 14.7%, respectively.
- (3) The optimal air premix ratio is determined to be a humidity ratio of 50 g/kg dry air with an oxygen concentration of 23%. This combination ensures efficient fuel combustion, prevents excessive NO concentration at the furnace outlet, and effectively reduces the CO concentration at the furnace outlet.

Author Contributions: Conceptualization, H.W. and C.Z.; methodology, H.W., Z.L., X.Z. and R.Z.; writing, H.W., J.D. and S.Z.; project administration, X.Y., X.Z., R.Z. and H.W. All authors have read and agreed to the published version of the manuscript.

Funding: This research was supported by the Academic Research Projects of Beijing Union University (No. ZK20202305) and funded by R&D Program of Beijing Municipal Education Commission (No. KM202311417007), Academic Research Projects of Beijing Union University (No. ZK20202202 and No. ZK10202203), Changzhou Applied Basic Research Funding Program (CJ20235015).

Data Availability Statement: Data are contained within the article.

Conflicts of Interest: Author Ruijuan Zhang was employed by the Beijing Heating Group Shijingshan Branch. The remaining authors declare that the research was conducted in the absence of any commercial or financial relationships that could be construed as a potential conflict of interest.

References

1. Lai, X.J.; Ye, Z.H.; Xu, Z.Z.; Holmes, M.H.; Lambright, W.H. Carbon capture and sequestration (CCS) technological innovation system in China: Structure, function evaluation and policy implication. *Energy Policy* **2012**, *50*, 635–646. [CrossRef]
2. Jayamaha, L. *Energy-Efficient Building Systems: Green Strategies for Operation and Maintenance*; McGraw Hill Professional: New York, NY, USA, 2006.
3. Roiha, I.; Kaikko, J.; Jaanu, K.; Vakkilainen, E.K. Analysis of high flue gas recirculation for small energy conversion systems. *Appl. Therm. Eng.* **2014**, *63*, 218–226. [CrossRef]
4. Zhang, Z. *Experimental and Numerical Studies of Humid Air Diffusion Flames*; Graduate School of Chinese Academy of Sciences: Beijing, China, 2006.
5. Yang, Y.; Tao, J.; Song, X. Experimental investigation on saturated humid air low NO_x combustion. *Ind. Boil.* **2018**, *6*, 11–16.
6. Shi, B.; Hu, J.; Peng, H.; Satoru, I. Effects of internal flue gas recirculation rate on the NO_x emission in a methane/air premixed flame. *Combust. Flame* **2018**, *188*, 199–211. [CrossRef]
7. Zhang, Q.; Zhou, Z.; Zhang, J.; Liu, T.; Xiao, X. Influence of combustion air humidification on low nitrogen combustion performance of gas boilers. *Chem. Eng.(China)* **2024**, *52*, 1–6. Available online: <https://qikan.cqvip.com/Qikan/Article/Detail?id=7111904235> (accessed on 10 October 2024).
8. Boushaki, T.; Dhue, Y.; Selle, L.; Ferret, B.; Poinot, T. Effects of hydrogen and steam addition on laminar burning velocity of methane-air premixed flame-Experimental and numerical analysis. *Int. J. Hydrogen Energy* **2012**, *37*, 9412–9422. [CrossRef]
9. Ge, B.; Tian, Y.; Xie, Y.; Zang, S.; Shu, S. Influence of humidity on a double swirled non-premixed syngas burner. *J. Shanghai Jiao Tong Univ.* **2014**, *48*, 746–749.
10. Yang, X.; Wei, W. Numerical simulation of combustion characteristics of a corner-tube gas boiler. *Comput. Sci. Eng.* **2018**, 347–352. [CrossRef] [PubMed]
11. Wang, J.; Zhao, Y.; Luo, Z.; Song, G.; Song, S.; Wang, P. Effects of different diluents on NO_x emission and combustion stability of boilers fueled by natural gas. *Environ. Eng.* **2019**, *37*, 148–153.
12. Mages, A.; Sauer, A. Comparison of the Temperature, Radiation, and Heat Flux Distribution of a Hydrogen and a Methane Flame in a Crucible Furnace Using Numerical Simulation. *Hydrogen* **2024**, *5*, 459–473. [CrossRef]

13. Sun, C.; Wang, T.; Wang, P.; Zhang, Y.; Cui, C.; Lu, Y.; Liu, W.; Zhang, Y.; Zhang, Y. Numerical Simulation and Field Experimental Study of Combustion Characteristics of Hydrogen-Enriched Natural Gas. *Processes* **2024**, *12*, 1325. [[CrossRef](#)]
14. Chen, Y.; Wang, J.; Zhang, J.; Li, Y. Numerical Study on Chemical Kinetic Characteristics of Counterflow Diffusion Flame Extinction of Methane/Ammonia/Air Flame under High Pressure or Air Preheating Temperature. *Molecules* **2024**, *29*, 3632. [[CrossRef](#)] [[PubMed](#)]
15. Li, Y.; Li, H.; Guo, H.; Li, Y.; Yao, M. A numerical investigation on methane combustion and emissions from a natural gas-diesel dual fuel engine using CFD model. *Appl. Energy* **2017**, *205*, 153–162. [[CrossRef](#)]
16. Perpignan, A.A.V.; Sampat, R.; Gangoli Rao, A. Modeling Pollutant Emissions of Flameless Combustion with a Joint CFD and Chemical Reactor Network Approach. *Front. Mech. Eng.* **2019**, *5*, 63. [[CrossRef](#)]
17. Khodabandeh, E.; Moghadasi, H.; Pour, M.S.; Ersson, M.; Jönsson, P.G.; Rosen, M.A.; Rahbari, A. CFD study of non-premixed swirling burners: Effect of turbulence models. *Chem. Eng.* **2020**, *28*, 1029–1038. [[CrossRef](#)]
18. He, Z.; Wang, Q.; Yuan, J. *Thermal Fluid Numerical Calculation Methods and Applications*; Machinery Industry Press: Beijing, China, 2014; p. 9.
19. Zhou, L. *Numerical Simulation of Turbulent Two-Phase Flow and Combustion*; Tsinghua University Press: Beijing, China, 1991; p. 92.
20. Li, S. *Numerical Simulation and Experimental Research for Natural Gas Combustion Characteristic under O₂/CO₂ Atmosphere*; Changjiang University: Jingzhou, China, 2016; pp. 24–25.
21. Dong, Q.; Jiang, Y.; Qiu, R. Reduction and optimization of methane combustion mechanism based on PCAS and genetic algorithm. *Fire Sci.* **2014**, *23*, 41–49.
22. Li, S.L.; Jiang, Y.; Chen, W.T. Numerical analysis on characteristics of soot particles in C₂H₄/CO₂/O₂/N₂ combustion. *Chin. J. Chem. Eng.* **2013**, *21*, 238–245. [[CrossRef](#)]
23. Zhang, Y.D. *Simulation Study on Simplification of Chemical Kinetics Model and Soot Formation for Ethylene Flames*; Huazhong University of Science and Technology: Wuhan, China, 2011; pp. 4–5.
24. Guo, J. *Numerical Simulation of Flame Space in an Oxygenenriched Combustion Roller Kiln*; Wuhan University of Technology: Wuhan, China, 2014.
25. Zhao, D.; Yamashita, H.; Kitagawa, K.; Arai, N.; Furuhashi, T. Behavior and effect on NO_x formation of OH radical in Methane-air diffusion flame with steam addition. *Combust. Flame* **2002**, *130*, 352–360. [[CrossRef](#)]
26. Law, C. *Combustion Physics*; Cambridge University Press: Cambridge, UK, 2006.
27. Cen, K.; Yao, Q. *Advanced Combustion*; Zhejiang University Press: Hangzhou, China, 2002.
28. Zhou, J. *Biomass Energy Engineering and Technology*; China Forestry Press: Beijing, China, 2011.
29. Li, D.X.; Shi, P.H.; Wang, J.B. High-efficiency absorption of high NO_x concentration in water or PEG using capillary pneumatic nebulizer packed with an expanded graphite filter. *Chem. Eng. J.* **2014**, *237*, 8–15. [[CrossRef](#)]
30. Xiao, X. *Simulation Study on the Nitrogen Reduction Performance of Gas Boilers under the Combustion of Air Humidification and Air Staging*; Beijing Architecture University: Beijing, China, 2021.
31. Ying, Y.Y.; Liu, D. Effects of water addition on soot properties in ethylene inverse diffusion flames. *Fuel* **2019**, *247*, 187–197. [[CrossRef](#)]
32. Zhu, Q.; Niu, Y.; Chen, X. The effect of water vapor on soot formation in laminar methane/air diffusion flame. *J. Saf. Environ.* **2017**, *17*, 174–177.

Disclaimer/Publisher's Note: The statements, opinions and data contained in all publications are solely those of the individual author(s) and contributor(s) and not of MDPI and/or the editor(s). MDPI and/or the editor(s) disclaim responsibility for any injury to people or property resulting from any ideas, methods, instructions or products referred to in the content.